Brain Topography (2022) 35:66–78
https://doi.org/10.1007/s10548-021-00862-0

ORIGINAL PAPER

Probing the Functional and Structural Connectivity Underlying EEG Traveling Waves

Yun Qin[1,3] · Nan Zhang[1] · Yan Chen[1] · Yue Tan[1] · Zhenglin Yang[4] · Yi Shi[4] · Cheng Luo[1,2] · Tiejun Liu[1,2,3] · Dezhong Yao[1,2,3]

Received: 16 July 2020 / Accepted: 27 June 2021 / Published online: 21 July 2021

Abstract

Neural oscillations play an important role in the maintenance of brain function by regulating multi-scale neural activity. Characterizing the traveling properties of EEG is helpful for understanding the spatiotemporal dynamics of neural oscillations. However, traveling EEG based on non-invasive approach has little been investigated, and the relationship with brain intrinsic connectivity is not well known. In this study, traveling EEG of different frequency bands on the scalp in terms of the center of mass (EEG-CM) was examined. Then, two quantitative indexes describing the spatiotemporal features of EEG-CM were proposed, i.e., the traveling lateralization and velocity of EEG-CM. Further, based on simultaneous EEG-MRI approach, the relationship between traveling EEG-CM and the resting-state functional networks, as well as the microstructural connectivity of white matter was investigated. The results showed that there was similar spatial distribution of EEG-CM under different frequency bands, while the velocity of rhythmic EEG-CM increased in higher frequency bands. The lateralization of EEG-CM in low frequency bands (< 30 Hz) demonstrated negative relationship with the basal ganglia network (BGN). In addition, the velocity of the traveling EEG-CM was associated with the fractional anisotropy (FA) in corpus callosum and corona radiate. These results provided valid quantitative EEG index for understanding the spatiotemporal characteristics of the scalp EEG, and implied that the EEG dynamics were representations of functional and structural organization of cortical and subcortical structures.

Keywords Traveling EEG · Spatiotemporal dynamics · Center of mass · Simultaneous EEG-MRI · Quantitative EEG

Introduction

Neural oscillations play an important role in the maintenance of brain function by regulating multi-scale neural activity (Fries 2005; Jacobs et al. 2007). The spatiotemporal patterns of rhythmic EEG represented how multiple brain regions recognize in different brain states (Brovelli et al. 2004; Cohen and X, 2017). Previous studies have examined the dynamic interactive characteristics of EEG by studying the point-to-point connections within local network or between different regions (Palva and Palva 2007; Tort et al. 2008). Since these rhythmic oscillations were presented as continuous neural patterns in space and time (Freeman et al. 2000; Agarwal et al. 2014), characterizing the traveling properties of EEG may provide a novel approach for understanding the oscillation spatiotemporal dynamics.

Traveling EEG was usually characterized by spatially coherent oscillation in specific brain regions and temporally propagating across the time course (Zhang et al. 2018).

Handling Editor: Micah M. Murray.

This article belongs to the Topical Collection: Contemporary Challenges in M/EEG Modelling.

✉ Dezhong Yao
dyao@uestc.edu.cn

1 MOE Key Lab for NeuroInformation, The Clinical Hospital of Chengdu Brain Science Institute, University of Electronic Science and Technology of China, Chengdu, China

2 School of Life Science and Technology, Center for Information in Medicine, University of Electronic Science and Technology of China, Chengdu, P.R. China

3 Sichuan Institute for Brain Science and Brain-Inspired Intelligence, Chengdu, P.R. China

4 School of Medicine, University of Electronic Science and Technology of China, Chengdu, P.R. China

There were two hypotheses about the generation of traveling EEG: the first was that traveling EEG was associated with the corticocortical long axons conduction, with a speed of 5-15 m/s; the second was that the slower traveling EEG was generated from the relatively local and slow-propagation oscillations, with a speed less than 1 m/s (Hindriks et al. 2014). Previous studies of the mechanism of traveling EEG studies have mostly focused on the animal models or intracranial electrode recordings, and one common method was based on the phase lag between different neural populations or cortical electrodes, which was associated with stationarity of the maximum values of the field distributions. The characterizations including wave front shape, traveling direction, velocity, were often involved in terms of spatial dimensions. It was found that the propagation of EEG in visual and somatosensory cortex was functionally important to visual perception and movement (Rubino et al. 2006; Zanos et al. 2015). Moreover, EEG traveling was proposed associating with the short-range feedback in local cortex, and had mediation in the thalamocortical circuit (Halgren et al. 2019). Therefore, EEG traveling was considered as a key mechanism for guiding the spatial propagation of neural activity and computational processes across the brain (Ermentrout and Kleinfeld 2001). However, there has been little research on non-invasive traveling waves in human brain, mainly because the scalp EEG was greatly affected by attenuation and mingling of volume conduction. Therefore, instead of focusing on a region or a network, the center of mass (CM) was proposed to project all positive or negative sites in space onto a central site to characterize the global spatiotemporal dynamic of rhythmic EEG (Wackermann et al. 1993; Manjarrez et al. 2007). This method, commonly termed as vector averaging, has been used in a variety of studies in the context of spike activity to detect the source and the population firing patterns (Demas et al. 2003; Prentice et al. 2011; Hilgen et al. 2017). Moreover, quantitative indicators of EEG traveling, such as lateralization and velocity, may refine the dynamic patterns of neural oscillations in different brain state. The relationship with the resting-state functional and structural connectivity may provide basis for the traveling properties of scalp EEG.

Simultaneous EEG-fMRI has been valid approach to detect the neural representations and the BOLD correlations (Michel and Murray 2012). Resting-state networks were intrinsic functional network patterns of brain without external stimuli (Biswal et al. 1995), which provided basis to maintain stable brain function and respond rapidly to external inputs (De Luca et al. 2006; Fox et al. 2006; Greicius 2008). The lateralization of resting-state network helped to balance the resource allocation, and played an important role in cognitive processing and healthy brain development (Toga and Thompson 2003; Stark et al. 2008; Hugdahl and Westerhausen 2010). Moreover, asymmetry of scalp EEG rhythm has also been widely reported (Tomarken et al. 1992; Bolduc et al. 2003). As the scalp EEG was the summary of the cortical activity, we hypothesized that the spatiotemporal characteristics of the traveling EEG can be represented by the combination of certain intrinsic resting-state networks. Moreover, as the traveling EEG wave was associated with the corticocortical axons conduction, investigating the relationship between EEG traveling velocity and the white matter connectivity based on EEG-MRI fusion may provide potential information of structural foundation for the traveling scalp EEG.

In this study, we examined the EEG global spatiotemporal dynamics based on the EEG-CM in different frequency bands, and proposed two quantitative EEG indexes, the lateralization and traveling velocity. Moreover, using simultaneous EEG and MRI, the association between EEG-CM traveling and the combination of resting-state functional networks, as well as the white matter structural connectivity were investigated (Fig. 1).

Materials and Methods

Participants and Simultaneous EEG-MRI Acquisition

Sixty healthy participants (29 females; mean age: 23.8 years; standard deviation: 2.6 years) were recruited in simultaneous EEG-MRI recording. This study was performed according to the guidelines approved by the Ethics Committee of the University of Electronic Science and Technology of China (UESTC). MRI data were collected using a 3-T MRI scanner

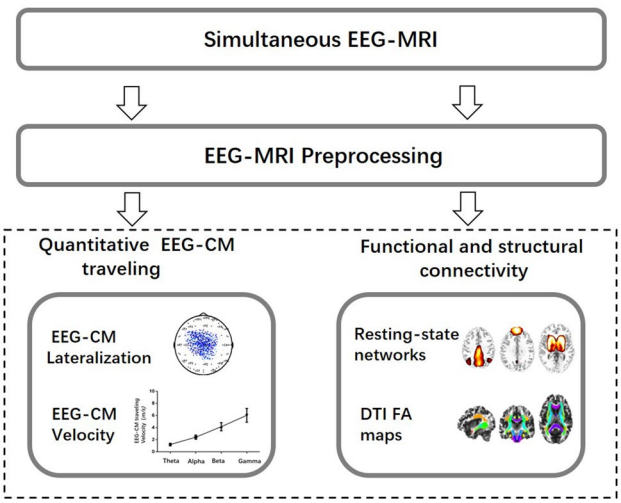

Fig. 1 Diagram of the EEG-MRI fusion in this study. After the processing of the quantitative EEG-CM traveling, fMRI-based resting-state network, and dMRI-based FA maps, the relationship between EEG-CM traveling and the functional / structural connectivity was calculated

(Discovery MR750, GE) in the Center for Information in Medicine of UESTC. High-resolution T1-weighted images were acquired using a 3- dimensional fast spoiled gradient echo (T1-3D FSPGR) sequence (TR / TE = 5.936 ms / 1.956 ms, flip angle [FA] = 9°, matrix = 256 × 256, field of view [FOV] = 25.6 × 25.6 cm^2, slice thickness = 1 mm, no gap, 152 slices). In addition, diffusion MRI (dMRI) data were acquired using a diffusion-weighted, spin-echo EPI sequence of 64 directions (2 × 2 × 2mm^3, FOV = 25.6 × 25.6 cm^2,TR / TE = 8500 ms / 70 ms, 76 slices, 64 directions, b=1000 s / mm^2).

Resting-state fMRI data were acquired using gradient-echo EPI sequences (TR / TE = 2000 ms / 30 ms, FA = 90°, matrix = 64 × 64, FOV = 24 × 24 cm^2, slice thickness/gap = 4 mm/0.4 mm), with an eight channel-phased array head coil. A 510 s resting-state scan was collected for each participant. Simultaneous EEG data were recorded using a 64-channel MR compatible EEG cap (Neuroscan, Charlotte, NC) according to the 10–20 standard system with a reference at the Fcz position. The amplifier (Neuroscan, synAmps2) was placed outside the scanning room, and the sampling rate was set at 5000 Hz. Electrode impedances were lowered to below 10 kΩ prior to recording. The EEG recording was synchronized with the MR scanner's internal clock to ensure the removal of the gradient artifacts in the EEG analyses. During the recording, all participants were instructed to close their eyes and relax without falling asleep.

EEG-MRI Data Preprocessing

All fMRI data were preprocessed using SPM12 (Statistical Parametric Mapping, http://www.fil.ion.ucl.ac.uk/spm/) and NIT (http://www.neuro.uestc.edu.cn/NIT.html) toolboxes. The first five volumes were discarded for the magnetization equilibrium from all fMRI scans. The remaining images were slice-time corrected, and spatially realigned to the first volume. All subjects have less than 2 mm for head movement and 2° for head rotation during MRI scanning. The individual T1 images were coregistered to the functional images, and then segmented and normalized to the Montreal Neurologic Institute (MNI) space. Then, functional images were spatially normalized using T1-based transformation, resampled to 3 × 3 × 3 mm^3 voxels, and spatially smoothed with a 6 mm full-width half maximum (FWHM) Gaussian kernel.

EEG data were preprocessed using Curry 7 software (Compumedics Neuroscan). MR gradient artifacts were removed by subtracting the averaged artifact template from the continuous EEG recordings based on the scanner triggers (Allen et al. 2000); then, the EEG data were bandpass filtered (1–45 Hz) and down-sampled to 250 Hz. Here, the bandpass filtering was based on an Infinite Impulse Response (IIR) band-pass filter. The ballistocardiogram (BCG) artifacts were corrected using the OBS-based BCG correction using the ECG channel (Niazy et al. 2005). Then, we used ICA to manually reject the movement-related and residual ballistocardiac artifacts. Finally, the preprocessed EEG were re-referenced to the neutral infinite reference using Reference electrode standardization technique (REST) (Yao 2001; Yao et al. 2019).

Preprocessing for dMRI data was carried out using FSL software (http://www.fmrib.ox.ac.uk/fsl/). First, dMRI images were visually inspected for image quality, and then corrected for eddy current and head motion by registering the diffusion weighted images to the b0 images. Next, a diffusion tensor model was fitted at each voxel to generate fractional anisotropy (FA) maps. After constructing the whole-brain voxel-wise diffusion parameter, individual b0 images were registered to the individual T1 images using rigid transformation. Then, individual dMRI images were normalized to the MNI standard space using the T1 transformation matrix. Based on the tract-based spatial statistics (TBSS), the transformed FA images of all participants were averaged to generate a mean FA image, and then thinned to create the white matter skeleton. A non-maximum suppression algorithm was applied to search the images voxels with the highest FA value along the direction perpendicular to the local tract surface to create a mean FA skeleton. A threshold setting at 0.2 was used to exclude the skelet on voxels probably containing the gray matter voxels. Finally, the normalized individual FA maps were projected to the mean FA skeleton to create individual skeletonized FA maps, which were used for the following EEG-MRI fusion analysis.

EEG-CM Quantitative Indicators: Traveling Velocity and Lateralization

In this study, positive CM was calculated with the following equations based on the weighted vector averaging method (Manjarrez et al. 2007). For each time point, the EEG amplitude of all channels formed the vector $m_i(t)$, and CM is calculated by the position-weighted average of the EEG data with positive amplitude.

$$\begin{aligned} x(t) &= \frac{\sum A_i m_i(t)}{\sum m_i(t)}, \quad m_i(t) > 0, \ \ i = 1 \ldots .N \\ y(t) &= \frac{\sum B_i m_i(t)}{\sum m_i(t)}, \quad m_i(t) > 0, \ \ i = 1 \ldots .N \\ z(t) &= \frac{\sum C_i m_i(t)}{\sum m_i(t)}, \quad m_i(t) > 0, \ \ i = 1 \ldots .N \end{aligned} \tag{1}$$

where $x(t)$, $y(t)$ and $z(t)$ are the orthogonal coordinates of CM; A_i, B_i and C_i are the coordinates of the electrode channel i; and $m_i(t)$ is the positive voltage of channel i at time point t; and N is the electrode number.

Here, we calculated the EEG-CM of different frequency bands, theta (4-7 Hz), alpha (8-12 Hz), beta (13-30 Hz), and gamma band (31-45 Hz). According to the instantaneous EEG-CM, two quantitative indicators were obtained, i.e., EEG-CM traveling velocity and traveling lateralization.

EEG-CM Traveling Velocity

The traveling velocity of EEG-CM at time point t was computed based on the Euclidean distance between the orthogonal coordinate of EEG-CM at this time point t and that at the prior time point t-1. Considering the fact that the source of scalp EEG is more likely located in the surface of the grey matter, we calculated the CM traveling velocity in the two-dimensional scalp field:

$$V(CM(t)) = \sqrt{(x(t) - x(t-1))^2 + (y(t) - y(t-1))^2}/dt \quad (2)$$

To calculate the quantitative traveling velocity, we normalized the electrode coordinates to the head model with the sphere radius r = 10 cm. Combing the sampling rate of the CM trajectory (i.e., 250 Hz in this analysis), the quantitative CM traveling velocity, i.e., m/s, was obtained.

EEG-CM Traveling Lateralization

EEG-CM lateralization was obtained based on the traveling trajectory across left and right hemisphere. The perpendicular distance from the EEG-CM to the center on the scalp formed the traveling trajectory sequence of the whole-time course (here, the center was set as the sagittal plane of midline), with the positive values when EEG-CM traveling in the left hemisphere and negative values when EEG-CM traveling in the right hemisphere. Then, the lateralization of EEG-CM was calculated based on the following formula:

$$B_{CM} = \frac{L(CM) - R(CM)}{L(CM) + R(CM)} \quad (3)$$

Here, $L(CM)$and$R(CM)$were the area under the curve (AUC) of the traveling trajectory sequence on the left and right hemisphere across the whole-time course, that is, the AUC of the positive values and AUC of the negative values. Then, the individual EEG-CM lateralization was obtained.

FMRI-Based Resting-State Network Lateralization

FMRI-based resting-state networks (RSNs) were obtained according to spatial independent component analysis (ICA). Group ICA was conducted in GIFT version 4.0a (Calhoun et al. 2011) (http://mialab.mrn.org/software/gift/). ICA decomposition generated independence components (ICs) with spatially non-overlapping and temporally coupled regions, and these regions formed a group of brain intrinsic network patterns. The estimation of ICs was repeated 20 times in ICASSO (http://research.ics.tkk.fi/ica/icasso), and the number of independent components (ICs) was determined by the Minimum description length (MDL) (Li et al. 2007). RSNs were identified based on the average power spectra and spatial pattern of the components (Luo et al. 2012).The individual spatial maps and their related time courses were acquired using dual-regression back-construction method, and the participant-specific maps were converted to Z-scores.

Then, standard MNI template was used to make a symmetrized template using the warping step, and the spatial maps of RSNs of all subjects were normalized to this symmetrized template. The group-level spatial maps of the normalized RSNs (one-sample t-test, $P < 0.01$, FDR corrected) were used as the mask, and the lateralization of the RSNs was calculated using the following formula:

$$B_{network} = \frac{L(network) - R(network)}{L(network) + R(network)} \quad (4)$$

Here, $L(network)$and$R(network)$was the sum of the values in left and right hemisphere for one certain RSN, respectively.

Multivariate Regression for EEG-CM and Resting-State Network Lateralization

In order to evaluate the relationship of EEG-CM traveling lateralization with the RSNs, we used a multivariate regression to link EEG-based and fMRI-based lateralization index:

$$Y = X\beta + \varepsilon \quad (5)$$

Here$Y = [y_1, y_2 \ldots, y_n]^T$denoted the lateralization of EEG-CM of all subjects, i.e.,B_{CM}, and $X = [X_1, X_2, \ldots, X_n]^T$ was the explanatory variable consisting of the lateralization of the RSNs of all subjects, where $X_i = [x_1, x_2, \ldots, x_m]$ denoted that subject i had m features in terms of RSNs, and$\beta = [\beta_1, \beta_2, \ldots, \beta_m]^T$was the parameter of the regression model relative to the explanatory variable; $\varepsilon$was the residual error.

After the parameters of the linear model was estimated by the ordinary least square method, the statistic test was carried out on the linear model (F-test), and student t test was also conducted to all the estimated parameters$\beta = [\beta_1, \beta_2, \ldots, \beta_m]^T$. This analysis gave us the optimized combination of RSNs that was significantly linearly correlated with the EEG-CM lateralization.

Covariation Between EEG-CM Traveling Velocity and DTI-Based FA Maps

Correlation analysis was performed between the FA maps and EEG-CM traveling velocity across subjects. Thus, the

voxels of WM fiber that are significantly related to EEG-CM traveling velocity were obtained ($P < 0.05$, FDR corrected).

Results

Resting-State EEG-CM Dynamics

After projecting the EEG-CM on the 2D head surface, it was found that the trajectory of all frequency bands on the scalp was mostly concentrated in the central area. Figure 2 illustrated a segment of EEG-CM trajectory (20 s) on the head scalp. The points demonstrated the traveling location of EEG-CM, and the size and color represented the traveling velocity of EEG-CM at this moment. Then, the averaged traveling velocity across the time course for different frequency bands was compared using the one-way repeated measurement analysis of variance (ANOVAs). The results showed that there was significant difference of EEG-CM traveling velocity among different bands ($P < 0.001$). Moreover, the EEG-CM traveling velocity enhanced with the higher frequency bands. Theta band demonstrated much lower traveling velocity, at about 1.2 m/s in group-level. The averaged velocity of alpha band in group-level was about 2.4 m/s, while the averaged velocity of beta and gamma band can reach 4 m/s and 6 m/s, respectively (Fig. 2b).

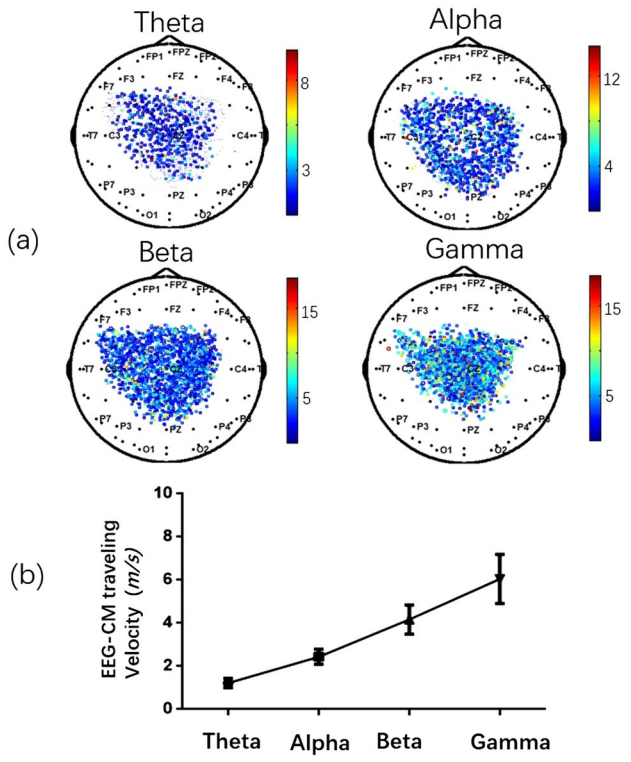

Fig. 2 The rhythmic EEG-CM traveling trajectory and velocity. **a** Illustration of EEG-CM traveling trajectory in different frequency bands. **b** Averaged EEG-CM traveling velocity in different frequency bands

Resting-State Networks and Relationship with Lateralization of EEG-CM

Twelve components were selected as the RSNs from group ICA processing. In accordance with the previously published results (Smith et al. 2009; Luo et al. 2012), these networks were labeled as follows: (1) SMN: sensorimotor network, including the pre- and post-central gyrus, paracentral lobule, and supplementary motor area; (2) VN: the primary visual network, consisting of the cuneus, calcarine, and lateral lingual gyrus; (3) AN: the auditory network, consisting of the middle temporal gyrus, superior temporal gyrus; (4) cerebellum: primarily encompassing the cerebellum posterior lobe and declive; (5) pDMN: the posterior part of default mode network (pDMN,) involving the posterior cingulate cortex (PCC), precuneus, and bilateral angular gyrus; (6) BGN: basal ganglia network, involving pallidum, caudate, putamen nucleus and part of thalamus and the parahippocampal gyrus; (7) aDMN: the anterior part of DMN (aDMN) including the superior frontal gyrus and middle frontal gyrus; (8) SN: the salience network, consisting of dorsal anterior cingulate (dACC) and orbital frontoinsular cortices, as well as part of prefrontal areas; (9) LFPN: the left lateral frontoparietal network involving the left middle frontal gyrus, inferior parietal lobule, superior parietal lobule and angular gyrus; (10) RFPN: the right lateral frontoparietal network showing the similar spatial patterns with LFPN; (11) DAN: dorsal attention network, mainly including the bilateral intraparietal sulcus, frontal eye field and middle temporal lobe; (12) CEN: the central executive network comprising the superior and middle frontal cortices, anterior cingulate and paracingulate gyri. The spatial patterns of the RSNs were shown in Fig. 3. Then, we calculated the lateralization of the RSNs, and the maps of $B_{network}$ in the group level based on one-sample *t*-test were illustrated in the Supplemental Materials (SFig. 1). There was a trend of leftward asymmetry in cortical networks such as DMN, DAN, and subcortical networks involving cerebellum, and BGN.

To detect how the EEG-CM lateralization was interpreted by the lateralization of resting-state intrinsic networks, the multivariate linear regression between them was performed. We adopted the statistical significance in *F*-test for the linear regression model ($P < 0.05$, Bonferroni-corrected), and *t*-test for the parameters ($P < 0.05$, non-corrected). The results showed that EEG-CM lateralization in theta band was negatively correlated with BGN and SN. Lateralization of EEG-CM in alpha band was negatively correlated with BGN and cerebellum network, and positively correlated with VN simultaneously.

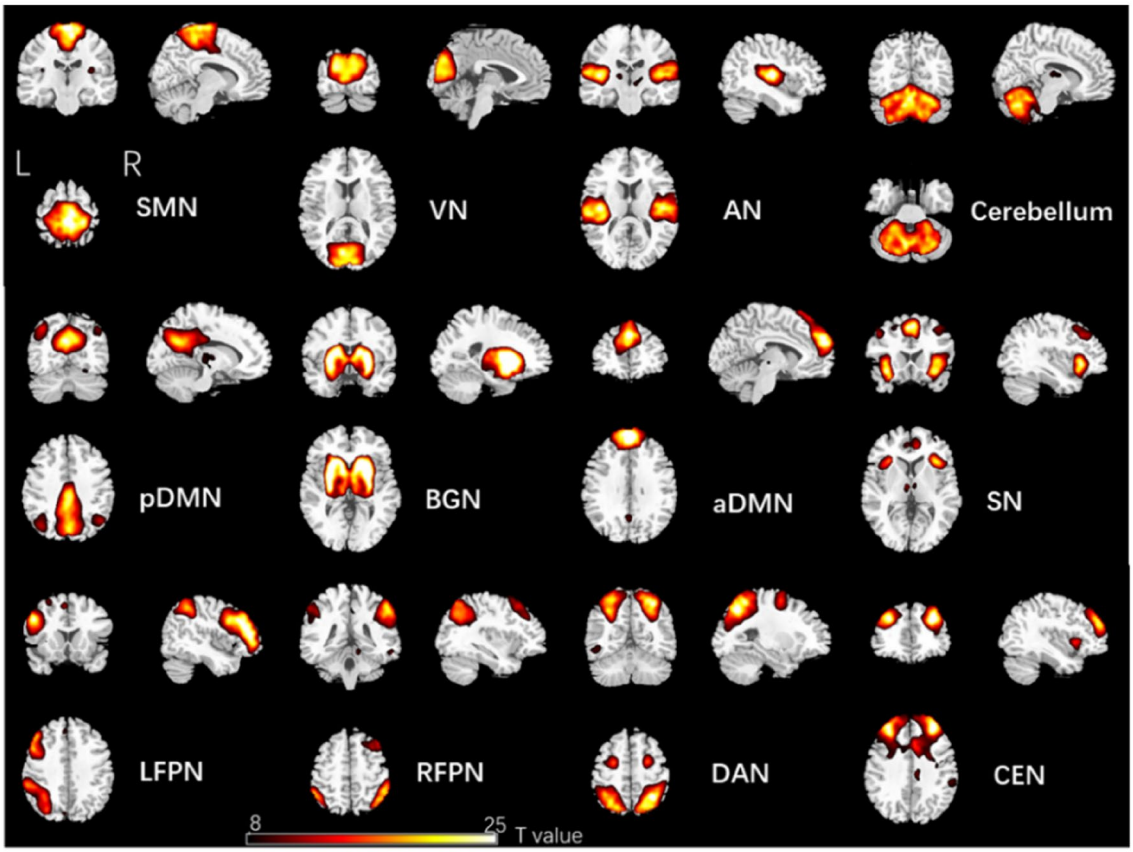

Fig. 3 The spatial patterns of 12 RSNs identified according to the group ICA

EEG-CM in beta band demonstrated negative correlation with BGN and pDMN (Fig. 4). No significant correlation was found between EEG-CM in gamma band and RSNs.

Covariation Between EEG-CM Traveling Velocity and DTI-Based FA Maps

Correlation between EEG-CM traveling velocity and FA maps was carried out across subjects. It was found that rhythmic EEG-CM traveling velocity was associated with FA values of certain white matter fibers. Generally, corpus callosum (CC) and corona radiata (CR) were dominated fiber bundles which were correlated with EEG-CM traveling velocity (Fig. 5; Table 1). In theta band, EEG-CM velocity was negatively correlated with the FA values in CC, deep frontal white matter, and positively correlated with a few of superior CR. While EEG-CM velocity in alpha band demonstrated distinct positive correlation with CC. The results in beta mainly included the negative correlation with posterior CR and deep frontal white matter, as well as the positive correlation with CC. As to gamma band, the positive correlation with EEG-CM velocity was located in CC and superior CR.

Discussion

In this study, we proposed two quantitative indexes, EEG-CM traveling lateralization and traveling velocity, to measure the global spatiotemporal characteristics of scalp EEG. Moreover, according to the simultaneous EEG-MRI fusion, EEG-CM traveling lateralization in low-frequency bands represented negative correlation with BGN. In addition, the relationship with corpus callosum and corona radiata implied the structural connectivity associated with the EEG spatiotemporal dynamics.

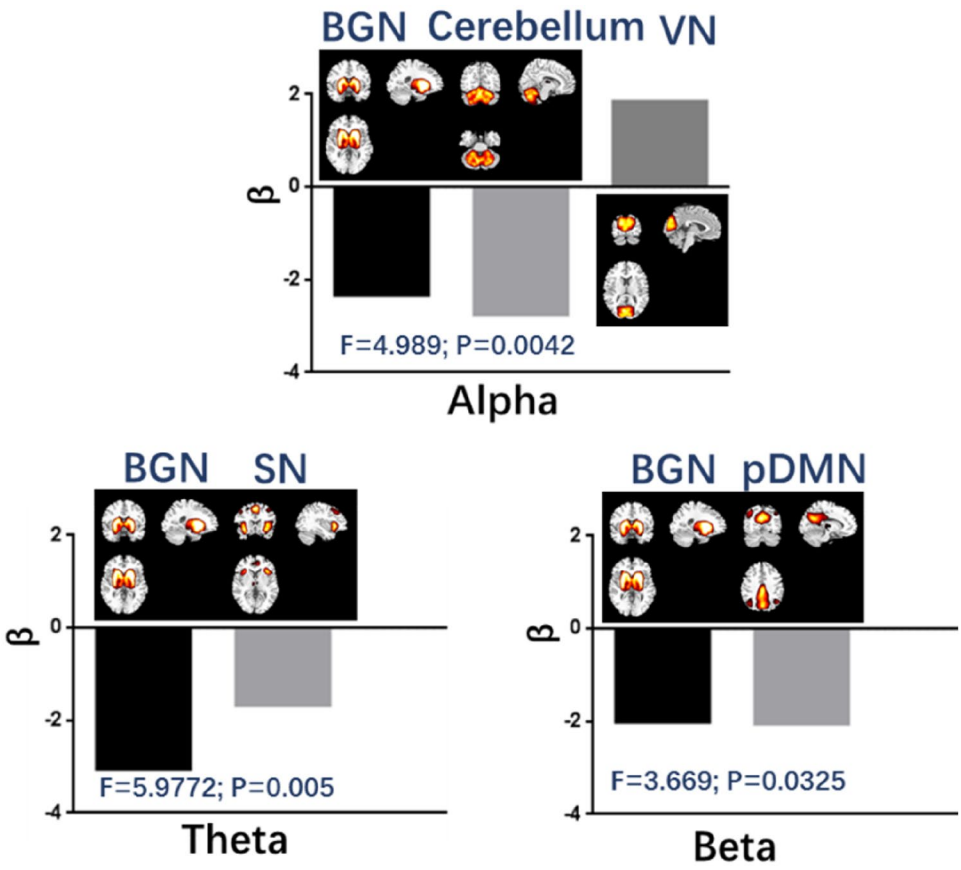

Fig. 4 The relationship between EEG-CM lateralization and the resting-state networks. The intrinsic networks which were linearly related with the rhythmic EEG-CM lateralization, and the parameters (β values) in the regression model were illustrated ($P < 0.05$)

Based on the vector averaging approach, EEG-CM was usually used to detect the patterns of neuronal activity in early studies (Demas et al. 2003; Prentice et al. 2011). In fact, EEG-CM was regarded as an epitome of the spectral topography according to spatial filtering. Most of EEG traveling waves were obtained from the invasive measurements based on intracranial EEG or electrocorticographic (ECoG) recordings, such as calculating phase lag between different neural populations or cortical electrodes. The characteristics including traveling direction, velocity, as determined by baseline crossing lags and peak lags in conventional EEG traces described the spatial gradient, which were associated with stationarity of the maximum values of the field distributions. However, due to the volume conduction effect of scalp EEG recording, it was not easy to investigate the spatial effect using the common measurements of traveling patterns, such as traditional phase synchronization, etc. In this article, we focused on the temporally dynamic CM representation, and the spatial topology was turned into a point in 2-dimensional space, which can more simply describe EEG dynamics in time. The results showed that EEG-CM trajectory in resting-state was concentrated near the center of the head, which may indicate the continuous characteristics of the spectral patterns covering the whole brain in the resting-state (Freeman et al. 2000). Here, resting-state EEG-CM traveling was not linked with cognitive function, but provided quantitative information, such as the traveling lateralization and velocity. In terms of traveling velocity, theta and alpha bands represented much lower velocity around 2 m/s, while beta and gamma demonstrated higher EEG-CM velocity around 5 m/s. Previous studies proposed that low-frequency bands were dominant in long-range communication, while high frequency bands were more involved in the communication of local brain regions (von Stein and Sarnthein 2000; Daume et al. 2017). Therefore, more stable spatiotemporal patterns of scalp EEG in low-frequency bands may be associated with the inter-regional interactions, while these interactions could be denoted by the intrinsic resting-state networks.

As expected, the traveling lateralization of EEG-CM can be linearly described by the combination of resting-state networks. For the low-frequency bands, i.e., theta, alpha and beta band, EEG-CM traveling lateralization was negatively correlated with the lateralization of BGN. BGN, as the main subcortical network of brain, was connected with the distributed cortical regions through the striatum pathway, and regulated cortical rhythmic oscillations and functional connectivity through thalamocortical projection (Ebner et al. 2015). The closed-loop circuit between BGN and neocortex, as well as between BGN and other subcortical structures, provided the basis for resource allocation

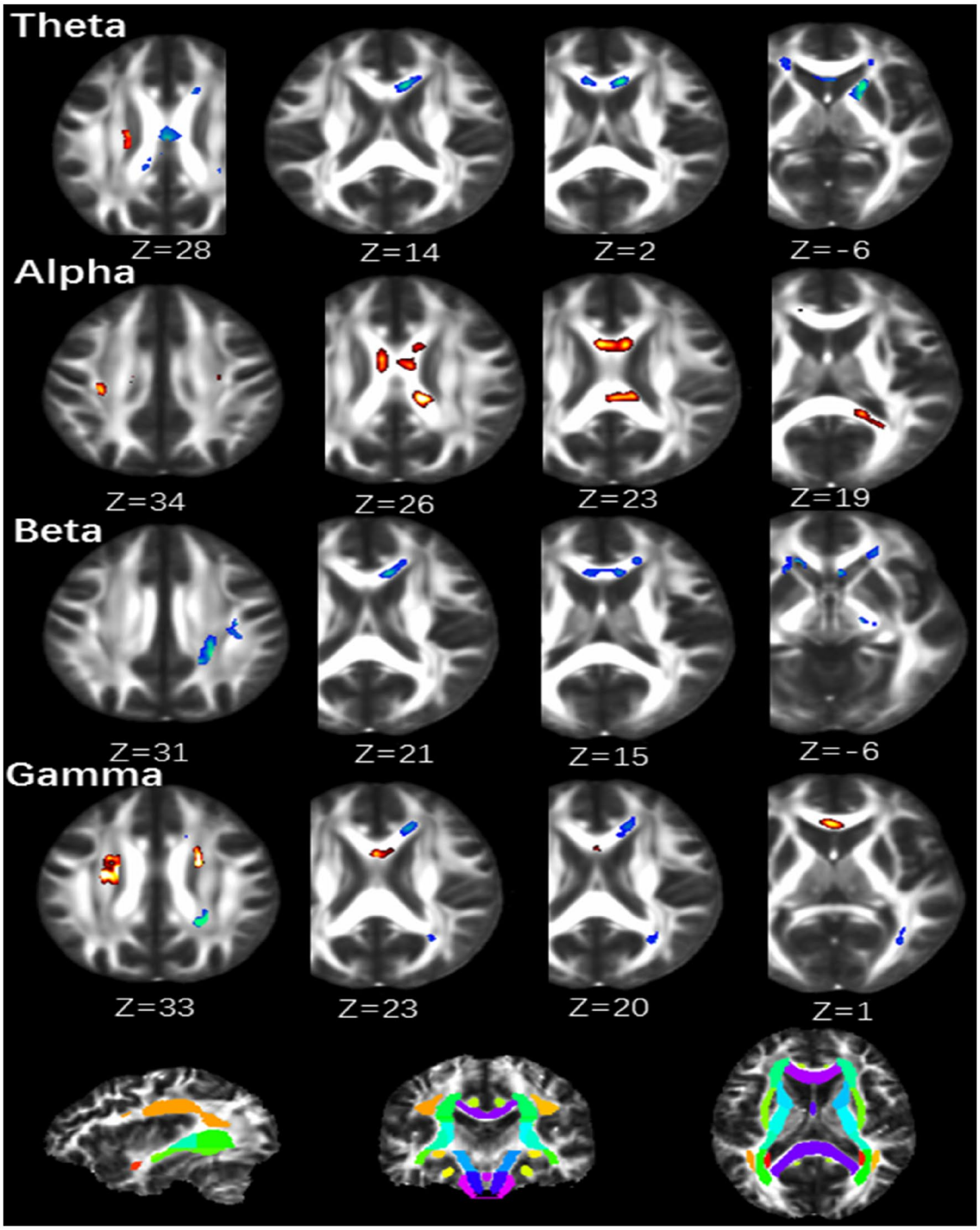

Fig. 5 The relationship between rhythmic EEG-CM traveling velocity and the FA values of white matter fibers ($P < 0.05$, FDR corrected). The voxels with the red color demonstrate the positive correlation voxels, and those with the blue color demonstrates the negative correlation. The bottom row is the white matter skeleton atlas with different color denoting 48 skeleton regions

and parallel processing of multiple information systems (Mchaffie et al. 2005). Therefore, the competition and conflict resolution strategies of the brain embodied by BGN had important significance for behavior selection. Due to the role of low-frequency rhythm in attention, cognitive control and long-range communication (Ward 2003), the relationship with BGN may indicate the negative modulation of subcortical regions through lateral regulation of cortical oscillations. In this study, the group-level of resting-state EEG-CM tended to be right lateralization, while a lot of functional

Table 1 The white matter fibers showing correlation with EEG-CM traveling velocity ($P < 0.05$, FDR-corrected)

MNI coordinate				
White matter fibers	X	Y	Z	R-value
Theta				
Superior corona radiata_L	−23	−18	29	0.3682
Body of corpus callosum	0	−14	28	−0.4166
Genu of corpus callosum	9	22	18	−0.3945
Anterior limb of internal capsule	21	17	4	−0.3792
Deep frontal whiter matter	−19	28	−6	−0.375
Alpha				
Superior corona radiata_L	−32	−19	35	0.3327
Body of corpus callosum	0	9	23	0.3984
Splenium of corpus callosum	14	−33	28	0.3091
Beta				
Posterior corona radiata_R	24	−40	33	−0.2933
Genu of corpus callosum	0	29	6	0.4027
Deep frontal whiter matter	17	26	21	−0.324
Gamma				
Superior corona radiata L	−24	−8	32	0.4255
Superior corona radiata_R	24	2	32	0.4032
Body of corpus callosum	4	6	23	0.3768
Frontal white matter	18	28	23	−0.3453
Parietal white matter	22	−38	35	−0.3288
Posterior thalamic radiation	34	−57	4	−0.4532

networks demonstrated left lateralization. This functional lateralization may be associated with the structure lateralization (Raz et al. 1995; Yamashita et al. 2011; Wyciszkiewicz and Pawlak 2014). In the previous studies, the structural lateralization was investigated in normal and abnormal brains based on the volume calculation and statistical analysis. The results mainly focused on certain brain regions, including the cortical and the subcortical regions. In normal brain, the rightward asymmetry was reported in the frontal areas, and the left asymmetry was found in parietal areas. However, the results on lateralization of regional volumes for subcortical regions such as caudate nucleus, thalamus, putamen were so far controversial. In our results, although we didn't detect the structural lateralization, we found dominant leftward asymmetry in cortical networks such as DMN, DAN, as well as the subcortical networks involving cerebellum, and BGN. In addition, EEG-CM lateralization of theta was also negatively related to SN network. SN was involved in the regulation of the whole brain by dynamically controlling the activities of other network (Seeley et al. 2007; Bonnelle et al. 2012), and presented a kind of adaptive regulation in the goal-directed top-down control (Miller and Cohen 2001). Therefore, SN played an important role in resource regulation and maintaining resource balance in cognitive tasks. The negative relationship between EEG-CM and SN lateralization may be related to the more concentrated resource invocation or less resource demand in the dominant hemisphere of SN. Similarly, pDMN network was also negatively related to EEG-CM in beta band. As the main network in resting-state, the deactivation of DMN acted upon the effective cognitive and behavior. The negative relationship may be also a result of cognitive resource balance. It was interesting that the cerebellum network represented a negative correlation with alpha lateralization, while the VN has a positive correlation with alpha lateralization. Previous study proposed that the circuit including cerebellum-BGN-cortical was associated with motor coordination, and this regulation was accompanied by synchronous alpha oscillation (Pollok et al. 2007). The positive correlation with VN reflected the close link between alpha and occipital regions. The enhanced alpha activity in dominant visual hemisphere may be associated with the inhibitory effect. Just like in visual attentional tasks, visual stimuli generated greater alpha suppression in the non-attentional hemisphere (Zumer et al. 2014). The lateralization of the response of VN is determined by the stimulus demand, and the inhibitory effect of alpha on the dominant VN in the resting-state may be conducive to information entering into the non-dominant hemisphere, thus playing an important role in the parallel processing of external perception.

Neural oscillations can regulate the neural activities of multiple scales, which was of great significance for the communication and functional integration of the brain (Wang 2010; Siegel et al. 2012). Previous studies found that neural oscillation propagated on the cortical or scalp with certain direction (Lubenov and Siapas 2009; Fellinger et al. 2012), and was thought to be the basis for information calculation in different regions (Ermentrout and Kleinfeld 2001). Also, the traveling characteristic of EEG was related to the individual behavior and cognitive functions. Most of the previous studies focused on the traveling wave of low-frequency band (Fellinger et al. 2012; Hindriks et al. 2014; Zhang et al. 2018). The propagation velocity of alpha oscillation on cortex was about 0.7-2.1 m/s, while the velocity on the scalp can reach to 5-15 m/s (Bahramisharif et al. 2013; Hindriks et al. 2014). The current study applied the temporal variation of EEG-CM to detect the traveling velocity, and the velocity range of these rhythmic oscillation was consistent with the previous studies (Massimini et al. 2004; Nunez and Srinivasan 2006; Manjarrez et al. 2007). The results demonstrated rhythmic EEG-CM traveling was associated with FA values of certain white matter fibers. The traveling velocity of EEG-CM in alpha band was significantly correlated with corpus callosum. As the main inter-hemisphere white matter fiber, the corpus callosum and the diffusion condition with high FA values may be the physical foundation of inter-hemisphere coherence of alpha oscillation (TenHouten et al. 1987; Vecchio et al. 2014). In addition, theta, beta and gamma bands had relationship with corona radiata. Corona radiata was the projection fiber from internal capsule to cerebral cortex, mainly connecting subcortical and cortical area. Clinical and somatosensory evoked potential studies has revealed that the corona radiata was also involved in the organization of the sensory and motor pathways (Kalita and Misra 1998).The relationship with rhythmic oscillation may indicate the modulation arising from subcortical structures to the cortex (Grillner et al. 2005; Giber et al. 2015).

Since EEG-CM was an epitome of the spectral topography, we conducted a complementary analysis and tried to investigate the relationship between the topography and the CM patterns. In terms of EEG topography, the common microstates of resting-state EEG were derived using global field power-based k-means clustering, and then, the CM patterns in each microstate were described on the scalp. The results were demonstrated in the Supplementary Materials (SFig. 2), and showed that there were different spatial patterns for each microstate. The predominant state with much longer duration was along with much lower CM traveling velocity. Moreover, we found that the traveling velocity was positively correlated with the microstate transition in theta and alpha band ($P < 0.05$). Therefore, although similar EEG-CM trajectories occur with different topographic distribution of microstates, the dynamic feature, i.e., traveling velocity, may be one potential valid representation of the brain activity. What's more, this univariate denoting the global spatiotemporal patterns of brain activity was more likely to link

with the functional and structural connectivity using MRI-based measurement.

Based on the simultaneous EEG-MRI, this study examined the functional and structural foundations of the traveling EEG-CM. However, there were several methodological limitations in this study. The first was the physiological meaning of EEG-CM, which was impossible to define the location of the source of scalp EEG. Based on the hypothesis that the temporal characteristics of the scalp EEG was reserved to a large extent, and the scalp EEG was spatially tangled because of the volume conduction effect, the quantitative characteristics of the traveling CM may be meaningful for understanding the dynamic patterns of the brain. That was the difference between this study and the traditional EEG traveling methods based on the phase lags and peak lags in EEG traces which can describe the spatial gradient. In addition, we used the standard sphere head model (r = 10 cm) and normalized electrode coordinates in the calculation of EEG-CM. However, individual electrode coordinates were helpful for accurate EEG-CM calculation. Finally, the EEG-MRI fusion was mainly based on the linear correlation across subjects. In the future studies, model driven method linking EEG features and MRI-based features in the same source space may provide additional information.

Conclusions

In conclusion, the study provided two quantitative indexes in terms of the EEG traveling wave. Based on the simultaneous EEG-MRI, the negative relationship between EEG-CM lateralization and BGN lateralization was demonstrated. In addition, the traveling velocity of EEG-CM was related to corpus callosum and corona radiata. The results implied that the EEG dynamics were valid representations of functional and structural organization of cortical and subcortical structures, and may be helpful for understanding the spatiotemporal characteristics of the scalp EEG.

Supplementary Information The online version contains supplementary material available at https://doi.org/10.1007/s10548-021-00862-0.

Acknowledgements This work was supported by grants from Sichuan Science and Technology Program (2020ZYD013), the National Nature Science Foundation of China (Grant Number: 81701778, 81771822, 81861128001, and 31771149), Guangdong Science and Technology Program (M172018B030339001).

Authors Contribution Conceived and designed the work: YQ, CL. Acquired the data: YQ, NZ, YC, YT, ZY, YS. Analyzed the data: YQ, NZ, YT. Wrote the paper: YQ, CL, DY. All authors revised the work for important intellectual content. All of the authors have read and approved the manuscript. Thanks to the two radiologists for the neuroimaging evaluation.

Data availability The datasets generated and analyzed during the current study are available from the corresponding author on reasonable request.

Declarations

Conflict of interest The authors declare that they have no conflict of interest.

References

Agarwal G, Stevenson IH, Berenyi A, Mizuseki K, Buzsaki G, Sommer FT (2014) Spatially distributed local fields in the hippocampus encode rat position. Science 344(6184):626–630. doi:https://doi.org/10.1126/science.1250444

Allen PJ, Josephs O, Turner R (2000) A method for removing imaging artifact from continuous EEG recorded during functional MRI. Neuroimage 12(2):230–239. https://doi.org/10.1006/nimg.2000.0599

Bahramisharif A, van Gerven MA, Aarnoutse EJ, Mercier MR, Schwartz TH, Foxe JJ et al (2013) Propagating neocortical gamma bursts are coordinated by traveling alpha waves. J Neurosci 33(48):18849–18854. doi:https://doi.org/10.1523/JNEUROSCI.2455-13.2013

Biswal B, Yetkin FZ, Haughton VM, Hyde JS (1995) Functional connectivity in the motor cortex of resting human brain using echo-planar MRI. Magn Reson Med 34(4):537–541. doi:https://doi.org/10.1002/mrm.1910340409

Bolduc C, Daoust AM, Limoges E, Braun CM, Godbout R (2003) Hemispheric lateralization of the EEG during wakefulness and REM sleep in young healthy adults. Brain Cogn 53(2):193–196. doi:https://doi.org/10.1016/s0278-2626(03)00108-8

Bonnelle V, Ham TE, Kinnunen RL, Mehta KM, Greenwood MA RJ, et al (2012) Salience network integrity predicts default mode network function after traumatic brain injury. Proc Natl Acad Sci USA 109(12):4690–4695. doi:https://doi.org/10.1073/pnas.1113455109

Brovelli A, Ding M, Ledberg A, Chen Y, Nakamura R, Bressler SL (2004) Beta oscillations in a large-scale sensorimotor cortical network: directional influences revealed by Granger causality. Proc Natl Acad Sci U S A 101(26):9849–9854. doi:https://doi.org/10.1073/pnas.0308538101

Calhoun VD, Thoma RJ, Teuscher U, Stevens M, Sadek JR, Phillips JP et al (2011) A Baseline for the Multivariate Comparison of Resting-State Networks. Frontiers in Systems Neuroscience. https://doi.org/10.3389/fnsys.2011.00002

Cohen, and X M (2017) Where Does EEG Come From and What Does It Mean? Trends Neurosci 40(4):208–218

Daume J, Gruber T, Engel AK, Friese U (2017) Phase-amplitude coupling and long-range phase synchronization reveal frontotemporal interactions during visual working memory. J Neurosci 37(2):313–322. https://doi.org/10.1523/JNEUROSCI.2130-16.2016

De Luca M, Beckmann CF, De Stefano N, Matthews PM, Smith SM (2006) fMRI resting state networks define distinct modes of long-distance interactions in the human brain. Neuroimage 29(4):1359–1367. doi:https://doi.org/10.1016/j.neuroimage.2005.08.035

Demas J, Eglen SJ, Wong RO (2003) Developmental loss of synchronous spontaneous activity in the mouse retina is independent of visual experience. J Neurosci 23(7):2851–2860

Ebner C, Schroll H, Winther G, Niedeggen M, Hamker FH (2015) Open and closed cortico-subcortical loops: A

neuro-computational account of access to consciousness in the distractor-induced blindness paradigm. Conscious Cogn 35:295–307. doi:https://doi.org/10.1016/j.concog.2015.02.007
Ermentrout GB, Kleinfeld D (2001) Traveling electrical waves in cortex: insights from phase dynamics and speculation on a computational role. Neuron 29(1):33–44. doi:https://doi.org/10.1016/s0896-6273(01)00178-7
Fellinger R, Gruber W, Zauner A, Freunberger R, Klimesch W (2012) Evoked traveling alpha waves predict visual-semantic categorization-speed. Neuroimage 59(4):3379–3388. doi:https://doi.org/10.1016/j.neuroimage.2011.11.010
Fox MD, Corbetta M, Snyder AZ, Vincent JL, Raichle ME (2006) Spontaneous neuronal activity distinguishes human dorsal and ventral attention systems. Proc Natl Acad Sci U S A 103(26):10046–10051. doi:https://doi.org/10.1073/pnas.0604187103
Freeman WJ, Rogers LJ, Holmes MD, Silbergeld DL (2000) Spatial spectral analysis of human electrocorticograms including the alpha and gamma bands. J Neurosci Methods 95(2):111–121. doi:https://doi.org/10.1016/s0165-0270(99)00160-0
Fries P (2005) A mechanism for cognitive dynamics: neuronal communication through neuronal coherence. Trends Cogn Sci 9(10):474–480. doi:https://doi.org/10.1016/j.tics.2005.08.011
Giber K, Diana MA, Plattner V, Dugue GP, Bokor H, Rousseau CV et al (2015) A subcortical inhibitory signal for behavioral arrest in the thalamus. Nat Neurosci 18(4):562–568. doi:https://doi.org/10.1038/nn.3951
Greicius M (2008) Resting-state functional connectivity in neuropsychiatric disorders. Curr Opin Neurol 21(4):424–430. doi:https://doi.org/10.1097/WCO.0b013e328306f2c5
Grillner S, Hellgren J, Menard A, Saitoh K, Wikstrom MA (2005) Mechanisms for selection of basic motor programs–roles for the striatum and pallidum. Trends Neurosci 28(7):364–370. doi:https://doi.org/10.1016/j.tins.2005.05.004
Halgren M, Ulbert I, Bastuji H, Fabo D, Eross L, Rey M et al (2019) The generation and propagation of the human alpha rhythm. Proc Natl Acad Sci U S A 116(47):23772–23782. doi:https://doi.org/10.1073/pnas.1913092116
Hilgen G, Sorbaro M, Pirmoradian S, Muthmann JO, Kepiro IE, Ullo S et al (2017) Unsupervised Spike Sorting for Large-Scale, High-Density Multielectrode Arrays. Cell Rep 18(10):2521–2532. doi:https://doi.org/10.1016/j.celrep.2017.02.038
Hindriks R, van Putten M, Deco G (2014) Intra-cortical propagation of EEG alpha oscillations. Neuroimage 103:444–453. doi:https://doi.org/10.1016/j.neuroimage.2014.08.027
Hugdahl K, Westerhausen R (2010) The Two Halves of the Brain. Springer, London
Jacobs J, Kahana MJ, Ekstrom AD, Fried I (2007) Brain oscillations control timing of single-neuron activity in humans. J Neurosci 27(14):3839–3844. doi:https://doi.org/10.1523/JNEUROSCI.4636-06.2007
Kalita J, Misra UK (1998) Somatosensory evoked potential studies in internal capsule and corona radiata infarction. J Neurol 245(8):531–536. doi:https://doi.org/10.1007/s004150050238
Li Y-O, Adalı T, Calhoun VD (2007) Estimating the number of independent components for functional magnetic resonance imaging data. Hum Brain Mapp 28:1251–1266. doi:https://doi.org/10.1002/hbm.20359. doi
Lubenov EV, Siapas AG (2009) Hippocampal theta oscillations are travelling waves. Nature 459(7246):534–539. doi:https://doi.org/10.1038/nature08010
Luo C, Qiu C, Guo Z, Fang J, Li Q, Lei X et al (2012) Disrupted Functional Brain Connectivity in Partial Epilepsy: A Resting-State fMRI Study. Plos One 7(1):e28196. doi:https://doi.org/10.1371/journal.pone.0028196
Manjarrez E, Vazquez M, Flores A (2007) Computing the center of mass for traveling alpha waves in the human brain. Brain research 1145:239–247. doi:https://doi.org/10.1016/j.brainres.2007.01.114
Massimini M, Huber R, Ferrarelli F, Hill S, Tononi G (2004) The sleep slow oscillation as a traveling wave. J Neurosci 24(31):6862–6870. doi:https://doi.org/10.1523/JNEUROSCI.1318-04.2004
Mchaffie JG, Stanford TR, Stein BE, Coizet V, Redgrave P (2005) Subcortical loops through the basal ganglia. Trends Neurosci 28(8):0–407
Michel CM, Murray MM (2012) Towards the utilization of EEG as a brain imaging tool. Neuroimage 61(2):371–385. doi:https://doi.org/10.1016/j.neuroimage.2011.12.039
Miller EK, Cohen JD (2001) An integrative theory of prefrontal cortex function. Annu Rev Neurosci 24:167–202. doi:https://doi.org/10.1146/annurev.neuro.24.1.167
Niazy RK, Beckmann CF, Iannetti GD, Brady JM, Smith SM (2005) Removal of FMRI environment artifacts from EEG data using optimal basis sets. Neuroimage 28(3):720–737. doi:https://doi.org/10.1016/j.neuroimage.2005.06.067
Nunez PL, Srinivasan R (2006) A theoretical basis for standing and traveling brain waves measured with human EEG with implications for an integrated consciousness. Clin Neurophysiol 117(11):2424–2435. doi:https://doi.org/10.1016/j.clinph.2006.06.754
Palva S, Palva JM (2007) New vistas for alpha-frequency band oscillations. Trends Neurosci 30(4):150–158. doi:https://doi.org/10.1016/j.tins.2007.02.001
Pollok B, Butz M, Gross J, Schnitzler A (2007) Intercerebellar coupling contributes to bimanual coordination. J Cogn Neurosci 19(4):704–719. doi:https://doi.org/10.1162/jocn.2007.19.4.704
Prentice JS, Homann J, Simmons KD, Tkacik G, Balasubramanian V, Nelson PC (2011) Fast, scalable, Bayesian spike identification for multi-electrode arrays. PLoS One 6(7):e19884. doi:https://doi.org/10.1371/journal.pone.0019884
Raz N, Torres IJ, Acker JD (1995) Age, gender, and hemispheric differences in human striatum: a quantitative review and new data from in vivo MRI morphometry. Neurobiol Learn Mem 63(2):133–142. doi:https://doi.org/10.1006/nlme.1995.1013
Rubino D, Robbins KA, Hatsopoulos NG (2006) Propagating waves mediate information transfer in the motor cortex. Nat Neurosci 9(12):1549–1557. doi:https://doi.org/10.1038/nn1802
Seeley WW, Menon V, Schatzberg AF, Keller J, Glover GH, Kenna H et al (2007) Dissociable intrinsic connectivity networks for salience processing and executive control. J Neurosci 27(9):2349–2356. doi:https://doi.org/10.1523/JNEUROSCI.5587-06.2007
Siegel M, Donner TH, Engel AK (2012) Spectral fingerprints of large-scale neuronal interactions. Nat Rev Neurosci 13(2):121–134. doi:https://doi.org/10.1038/nrn3137
Smith SM, Fox PT, Miller KL, Glahn DC, Fox PM, Mackay CE et al (2009) Correspondence of the brain's functional architecture during activation and rest. Proc Natl Acad Sci U S A 106(31):13040–13045. doi:https://doi.org/10.1073/pnas.0905267106
Stark DE, Margulies DS, Shehzad ZE, Reiss P, Kelly AM, Uddin LQ et al (2008) Regional variation in interhemispheric coordination of intrinsic hemodynamic fluctuations. J Neurosci 28(51):13754–13764. doi:https://doi.org/10.1523/JNEUROSCI.4544-08.2008
TenHouten WD, Walter DO, Hoppe KD, Bogen JE (1987) Alexithymia and the split brain. V. EEG alpha-band interhemispheric coherence analysis. Psychother Psychosom 47(1):1–10. doi:https://doi.org/10.1159/000287991
Toga AW, Thompson PM (2003) Mapping brain asymmetry. Nat Rev Neurosci 4(1):37–48. doi:https://doi.org/10.1038/nrn1009
Tomarken AJ, Davidson RJ, Wheeler RE, Kinney L (1992) Psychometric properties of resting anterior EEG asymmetry: temporal

stability and internal consistency. Psychophysiology 29(5):576–592. doi:https://doi.org/10.1111/j.1469-8986.1992.tb02034.x

Tort AB, Kramer MA, Thorn C, Gibson DJ, Kubota Y, Graybiel AM et al (2008) Dynamic cross-frequency couplings of local field potential oscillations in rat striatum and hippocampus during performance of a T-maze task. Proc Natl Acad Sci U S A 105(51):20517–20522. doi:https://doi.org/10.1073/pnas.0810524105

Vecchio F, Lacidogna G, Miraglia F, Bramanti P, Ferreri F, Rossini PM (2014) Prestimulus interhemispheric coupling of brain rhythms predicts cognitive-motor performance in healthy humans. J Cogn Neurosci 26(9):1883–1890. doi:https://doi.org/10.1162/jocn_a_00615

von Stein A, Sarnthein J (2000) Different frequencies for different scales of cortical integration: from local gamma to long range alpha/theta synchronization. Int J Psychophysiol 38(3):301–313. doi:https://doi.org/10.1016/s0167-8760(00)00172-0

Wackermann J, Lehmann D, Michel CM, Strik WK (1993) Adaptive segmentation of spontaneous EEG map series into spatially defined microstates. Int J Psychophysiol 14(3):269–283. doi:https://doi.org/10.1016/0167-8760(93)90041-m

Wang XJ (2010) Neurophysiological and computational principles of cortical rhythms in cognition. Physiol Rev 90(3):1195–1268. doi:https://doi.org/10.1152/physrev.00035.2008

Ward LM (2003) Synchronous neural oscillations and cognitive processes. Trends Cogn Sci 7(12):553–559. doi:https://doi.org/10.1016/j.tics.2003.10.012

Wyciszkiewicz A, Pawlak MA (2014) Basal ganglia volumes: mr-derived reference ranges and lateralization indices for children and young adults. Neuroradiol J 27(5):595–612. https://doi.org/10.15274/NRJ-2014-10073

Yamashita K, Yoshiura T, Hiwatashi A, Noguchi T, Togao O, Takayama Y et al (2011) Volumetric asymmetry and differential aging effect of the human caudate nucleus in normal individuals: a prospective MR imaging study. J Neuroimaging 21(1):34–37. doi:https://doi.org/10.1111/j.1552-6569.2009.00403.x

Yao DZ (2001) A method to standardize a reference of scalp EEG recordings to a point at infinity. Physiol Meas 22(4):693–711. doi:https://doi.org/10.1088/0967-3334/26/3/003

Yao DZ, Qin Y, Hu S, Dong L, Vega MLB, Sosa PAV (2019) Which reference should we use for EEG and ERP practice? Brain Topogr 32(4):530–549. https://doi.org/10.1007/s10548-019-00707-x

Zanos TP, Mineault PJ, Nasiotis KT, Guitton D, Pack CC (2015) A sensorimotor role for traveling waves in primate visual cortex. Neuron 85(3):615–627. doi:https://doi.org/10.1016/j.neuron.2014.12.043

Zhang H, Watrous AJ, Patel A, Jacobs J (2018) Theta and Alpha oscillations are traveling waves in the human neocortex. Neuron 98(6):1269-1281 e1264. https://doi.org/10.1016/j.neuron.2018.05.019

Zumer JM, Scheeringa R, Schoffelen JM, Norris DG, Jensen O (2014) Occipital alpha activity during stimulus processing gates the information flow to object-selective cortex. PLoS Biol 12(10):e1001965. doi:https://doi.org/10.1371/journal.pbio.1001965